

Theory of the unstable Bessel resonator

Raúl I. Hernández-Aranda

Photonics and Mathematical Optics Group, Tecnológico de Monterrey, Monterrey, México 64849

Sabino Chávez-Cerda

Instituto Nacional de Astrofísica, Óptica y Electrónica, Apartado Postal 51/216, Puebla, México 72000

Julio C. Gutiérrez-Vega

Photonics and Mathematical Optics Group, Tecnológico de Monterrey, Monterrey, México 64849

Received January 5, 2005; revised manuscript received March 2, 2005; accepted March 7, 2005

A rigorous analysis of the unstable Bessel resonator with convex output coupler is presented. The Huygens–Fresnel self-consistency equation is solved to extract the first eigenmodes and eigenvalues of the cavity, taking into account the finite apertures of the mirrors. Attention was directed to the dependence of the output transverse profiles; the losses; and the modal-frequency changes on the curvature of the output coupler, the cavity length, and the angle of the axicon. Our analysis revealed that while the stable Bessel resonator retains a Gaussian radial modulation on the Bessel rings, the unstable configuration exhibits a more uniform amplitude modulation that produces output profiles more similar to ideal Bessel beams. The unstable cavity also possesses higher-mode discrimination in favor of the fundamental mode than does the stable configuration.

© 2005 Optical Society of America

OCIS codes: 140.3300, 140.3410, 140.4780.

1. INTRODUCTION

In recent years, several ways to produce Bessel beams have been demonstrated; for instance, passive optical systems fed by laser light using a ring aperture and a positive lens,^{1,2} refractive or diffractive axicons,^{3,4} holographic methods,^{5,6} Fabry–Perot interferometers,⁷ or diffractive phase elements.⁸ Active schemes to produce Bessel-type modes in laser resonators have also been proposed: for example, arrangements based on annular intracavity elements,⁹ output mirrors with annular apertures to produce conical fields,¹⁰ graded-phase mirrors,¹¹ and diode-pumped Nd:YAG lasers.¹²

Axicon-based resonators supporting Bessel beams were proposed independently by Rogel-Salazar *et al.*¹³ and Khilo *et al.*¹⁴ in 2001. This configuration has the advantage that it does not require intracavity optics or special shapes of the active medium. In 2003, Gutiérrez-Vega *et al.*¹⁵ continued the exploration of the axicon-based resonator properties, extending the analysis to concave-spherical mirrors and developing a formal geometric and wave analysis of the performance of the bare cavity. The axicon-based resonator with a convex output coupler operating in an unstable regime was proposed by Tsangaris *et al.*¹⁶ in 2003. The scope of this initial work was restricted to the calculation of the output shape of the dominant Bessel mode using the classical iterative Fox–Li algorithm.^{17,18}

In this paper we present a rigorous analysis of the axicon-based unstable Bessel resonator (UBR). The configuration we consider presents two important modifications with respect to the conventional stable Bessel resonator (SBR) studied in Ref. 15, namely, the output mirror

is now convex spherical, and the aperture ratio between the output coupler and the conical mirror has been reduced from unity to one half. The Huygens–Fresnel integral self-consistency equation for the cavity is efficiently solved using a matrix technique. This method has two main advantages: It extracts the lowest N modes and their eigenvalues at one time, and its accuracy is determined by the order N of the matrix. In our analysis we account for the effects of the finite aperture size of the cavity mirrors. Additionally, the Fox–Li algorithm is employed to describe the three-dimensional intracavity field distribution of the dominant mode and also to confirm the results obtained with the Huygens–Fresnel integral approach.

We study the effects of varying the curvature of the output mirror and the cavity length on the output transverse profile, the loss, and the resonance frequency shift of the lower modes. The analysis reveals that both the spherical mirror and the cavity length can be modified to minimize the losses due to diffraction and to adjust the radial modulation of the Bessel rings of the output field. As seen in our results, the transition between the SBR and the UBR is characterized by a continuous change in the associated diffraction losses and frequency shifts. Higher-order-mode crossings in the eigenvalue spectrum of the resonator are also present for several values of the radius of curvature of the output coupler.

2. RESONATOR CONFIGURATION

The configuration of the UBR consists of a reflective conical mirror with characteristic angle θ_0 and a convex–

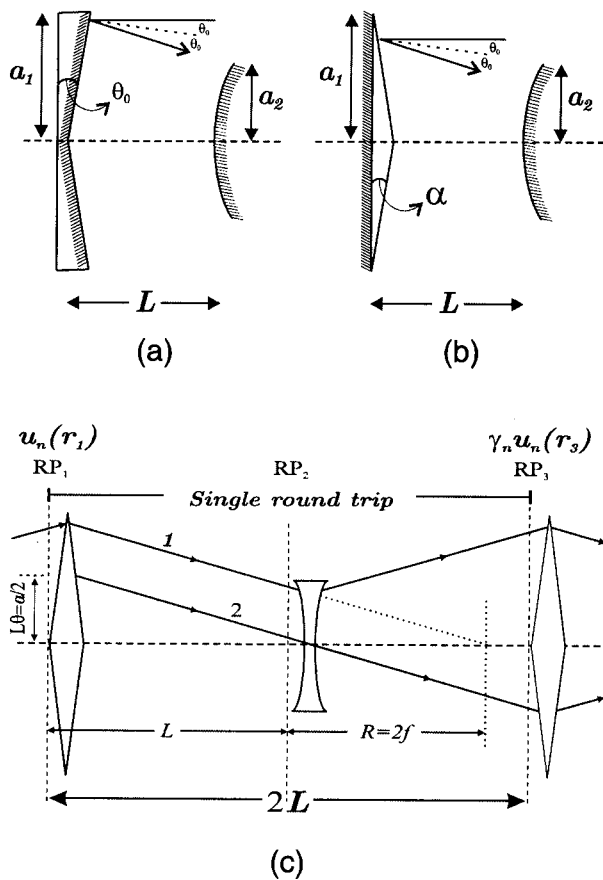


Fig. 1. Design of the resonator with (a) reflective and (b) refractive axicon. The convex-spherical mirror is placed at a distance L from the axicon. (c) Lens-guide-equivalent resonator and self-reproducibility condition for ray trajectories after one and two round trips. RP stands for reference plane.

spherical output mirror separated a distance L as depicted in Fig. 1(a). For the sake of generality, we will assume that the transverse radii of the conical mirror (a_1) and the output mirror (a_2) are independent and thus can take different values. The conical mirror transforms an incident plane wave into a converging conical wave. The trajectory of a horizontal input ray, except a ray that crosses through the center of the conical mirror, is always changed at a constant angle $2\theta_0$ toward the optical axis [see Fig. 1(a)]. In practice, the reflective conical mirror can also be constructed with a refractive axicon with index of refraction n and wedge angle α backed by a perfectly reflecting plane mirror, as shown in Fig. 1(b). In this case the conical angle θ_0 is related to the axicon parameters by $\theta_0 = \arcsin(n \sin \alpha) - \alpha \approx (n - 1)\alpha$, where the small-angle approximation $\sin \phi \approx \phi$ has been used. In contrast to the procedure in unstable resonators with two spherical mirrors, the laser output in the UBR is taken as a diffraction-coupled beam passing through (rather than around) the output mirror.

The cavity length is chosen to be

$$L = \frac{a_1}{2 \tan \theta_0} \approx \frac{a_1}{2 \theta_0} \quad (1)$$

to satisfy the requirement that the UBR reduces to the ideal SBR¹³ when the spherical output mirror becomes a flat mirror. The radius of curvature R of the output mirror is then a free parameter that can be used to modify the diffraction properties of the cavity.

The case $R > 0$ corresponds to a concave output coupler, for which the resonator is geometrically stable and the field at the output plane can be approximated by an l th order Bessel-Gauss beam,¹⁵

$$u(r) = J_l(k_t r) \exp\left(-\frac{r^2}{w^2}\right) \exp[i(l\phi + \Phi)], \quad (2)$$

where the waist w is given by $w^2 = w_0^2 [1 + (L/z_R)^2]$ with $w_0 = (2z_R/k)^{1/2}$, $z_R = [L(R-L)]^{1/2}$ is the Rayleigh range of the equivalent Gaussian beam, $\Phi = kr^2/2R$ is the phase of the spherical wave front at the output mirror, and $k_t = k \sin \theta_0$ is the transverse wave number. In the limit of a flat output coupler ($R \rightarrow \infty$), Bessel-Gauss modes reduce to Bessel beams $J_l(k_t \rho) \exp(il\phi)$. In real resonators the finite extent of the mirrors slightly modifies the transverse shape of the ideal Bessel modes such that, even in the case of a plane output mirror, the resonating modes are modulated by a bell-shaped envelope.

Output fields with specific transverse features can be generated by properly choosing the geometric parameters of the UBR in Fig. 1. As we will confirm in the remainder of the paper, under the paraxial regime and neglecting the finite size of the apertures, the output field may be approximated by the product of an ideal Bessel beam and the field produced by a half-symmetric unstable resonator in which one mirror is planar (axicon plane) and the other is convex (output plane). When considering the finite extent of the mirrors, the output function seems to be modulated by a near-top-hat function that is a good approximation of the ideal situation of having a constant amplitude modulation. As occurs in the SBR, the radial separation of the Bessel rings in the UBR will depend only on the angle θ_0 of the conical mirror.

A first useful picture, even if not fully detailed, of the mode properties of the UBR can be obtained from a purely geometric analysis. The equivalent lens-guide system of the UBR is shown in Fig. 1(c). The conical mirror is represented by a double refractive axicon whose $ABCD$ ray transfer matrix is written as

$$\begin{bmatrix} r_2 \\ \theta_2 \end{bmatrix} = \begin{bmatrix} 1 & 0 \\ -2\theta_0/r_1 & 1 \end{bmatrix} \begin{bmatrix} r_1 \\ \theta_1 \end{bmatrix}, \quad (3)$$

where (r_1, θ_1) and (r_2, θ_2) are the position and slope of the input and output rays, respectively.¹⁵ Note that the radius r is explicitly part of the $ABCD$ matrix for the double axicon and, eventually, of the self-consistency condition. With the reference planes placed just before the double axicon, the $ABCD$ matrix for the complete cavity is given by

$$\begin{bmatrix} A & B \\ C & D \end{bmatrix} = \begin{bmatrix} 1 & L \\ 0 & 1 \end{bmatrix} \begin{bmatrix} 1 & 0 \\ 2/R & 1 \end{bmatrix} \begin{bmatrix} 1 & L \\ 0 & 1 \end{bmatrix} \begin{bmatrix} 1 & 0 \\ -2\theta_0/r_1 & 1 \end{bmatrix} \quad (4a)$$

$$= \begin{bmatrix} 1 + \frac{2L}{R} + \left(-\frac{2\theta_0}{r_1}\right)2L\left(1 + \frac{L}{R}\right) & 2L\left(1 + \frac{L}{R}\right) \\ \left(-\frac{2\theta_0}{r_1}\right)\left(1 + \frac{2L}{R}\right) + \frac{2}{R} & 1 + \frac{2L}{R} \end{bmatrix}. \quad (4b)$$

We are interested in stable trajectories inside the cavity. The mathematical problem is that of finding the eigenvectors (r, θ) of the self-reproducibility equation

$$\begin{bmatrix} A & B \\ C & D \end{bmatrix} \begin{pmatrix} r \\ \theta \end{pmatrix} = \pm \begin{pmatrix} r \\ \theta \end{pmatrix}, \quad (5)$$

where the plus and minus signs correspond to trajectories that are self-reproducible after one and two round trips, respectively [see Fig. 1(c)]. Nonzero solutions are possible only if

$$\det \begin{bmatrix} A \mp 1 & B \\ C & D \mp 1 \end{bmatrix} = 0. \quad (6)$$

Taking advantage of the fact that $AD - BC = 1$, we can see that Eq. (6) vanishes only if $A + D = \pm 2$. By replacing A and D from Eq. (4b) into conditions $A + D = \pm 2$ and solving for r , we get the eigenvalues corresponding to self-reproducing trajectories after one and two round trips, respectively:

$$r_{\text{one}} = (L + R)\theta_0, \quad r_{\text{two}} = L\theta_0 = a_1/2. \quad (7)$$

As expected, the eigenangles θ associated with each r are found to be $\theta_{\text{one}} = \theta_{\text{two}} = \theta_0$. Note that r_{two} depends only on the aperture of the axicon, so it is always present in the cavity, but the existence of one round-trip stable trajectory is not always guaranteed because it depends on the radius of curvature of the output mirror.

In Fig. 1(c) we show the stable trajectories corresponding to one and two round trips. Note that the two round-trip trajectories always intersect the axicon plane at radius $r = a_2/2$ and the output mirror at its center.

3. WAVE-OPTICS ANALYSIS

A. Canonical Formulation of Unstable Bessel Resonators

The geometric description provides a useful but limited approximation to the mode properties of the UBR. A more detailed understanding of the mode distribution is obtained by solving the self-consistency Huygens–Fresnel integral equation for a given resonating mode.

In the equivalent lens-guide system shown in Fig. 1(c), the complete round trip inside the resonator can be broken into two segments. The first segment corresponds to the propagation from just before the double axicon (RP₁) to the output mirror (RP₂) and then to the original starting plane (RP₃).

The Huygens–Fresnel integral for the propagation of mode u_{lp} with azimuthal mode index $l=0, \pm 1, \pm 2, \dots$ and a radial mode index $p=1, 2, 3, \dots$ through a paraxial cy-

lindrical system from plane RP_m [coordinates (r_m, φ)] to plane RP_n [coordinates (r_n, φ)] is given by¹⁸

$$u_{lp}(r_n) = \int_0^{a_m} K_l(r_m, r_n) T_m(r_m) u_{lp}(r_m) dr_m, \quad (8)$$

where $T_m(r_m)$ is the transmittance function of the optical element or aperture located at plane RP_m, and the kernel $K_l(r_m, r_n)$ is defined in terms of the $ABCD$ elements for the propagation segment between the planes m and n , namely,

$$K_l(r_m, r_n) = (-i)^{l+1} \left(\frac{k}{B}\right) r_m J_l\left(\frac{k}{B} r_m r_n\right) \exp\left[\frac{ik}{2B}(Ar_m^2 + Dr_n^2)\right], \quad (9)$$

with $J_l(\cdot)$ being the l th-order Bessel function. In our case, the $ABCD$ elements correspond to the free-space propagation through a distance L , namely, $A=D=1$ and $B=L$. The upper limit in Eq. (8) corresponds to the radius of the aperture at RP_m.

The transmittance functions of the double axicon and the convex output mirror are given by

$$T_1(r_1) = \exp(-i2k\theta_0 r_1), \quad r_1 \leq a_1, \quad (10)$$

$$T_2(r_2) = \exp(-ikr_2^2/R), \quad r_2 \leq a_2, \quad (11)$$

where a time dependence $\exp(-i\omega t)$ has been assumed and irrelevant constant phase shifts have been ignored. Note that the double axicon exhibits a linear phase radial variation instead of the quadratic variation of the spherical lens. For generality, in the following analysis the radii of the double axicon and the output mirror can assume different numerical values.

The round-trip propagation for the UBR is described by the following pair of coupled integral equations^{19,20}:

$$u_{lp}(r_2) = \int_0^{a_1} K_l(r_1, r_2) T_1(r_1) u_{lp}(r_1) dr_1, \quad (12)$$

$$u_{lp}(r_3) = \int_0^{a_2} K_l(r_2, r_3) T_2(r_2) u_{lp}(r_2) dr_2. \quad (13)$$

By direct substitution of Eq. (12) into Eq. (13), we find the round-trip integral from RP₁ to RP₃,

$$u_{lp}(r_3) = \int_0^{a_1} H_l^{13}(r_1, r_3) u_{lp}(r_1) dr_1, \quad (14)$$

where we have used the fact that the radial coordinates in both planes are numerically the same, as illustrated in Fig. 1(c).

The kernel in Eq. (14) includes information about both propagation kernels in Eqs. (12) and (13) and the transmittance functions T_1 and T_2 . We have explicitly

$$H_l^{13}(r_1, r_3) = \int_0^{a_2} H_l^{23}(r_2, r_3) H_l^{12}(r_1, r_2) dr_2, \quad (15)$$

with $H_l^{12}(r_1, r_2) = K_l(r_1, r_2) T_1(r_1)$, $H_l^{23}(r_2, r_3) = K_l(r_2, r_3) \times T_2(r_2)$, where the superscripts (m, n) mean that the kernels are evaluated from RP_m to RP_n.

Finally, at the reference plane each eigenmode u_{lp} in the cavity satisfies the self-consistency integral equation

$$\gamma_{lp} u_{lp}(r_3) = \int_0^{a_1} H_l^{13}(r_1, r_3) u_{lp}(r_1) dr_1, \quad (16)$$

where the complex eigenvalue

$$\gamma_{lp} = |\gamma_{lp}| \exp(i\beta_{lp}) \quad (17)$$

defines the fractional power loss per transit

$$\Gamma_{lp} = 1 - |\gamma_{lp}|^2 \quad (18)$$

and the phase shift β_{lp} suffered by the mode in addition to the longitudinal phase shift kL . The resonant condition requires that the total phase shift Φ along the axis of the cavity be an entire multiple of π radians, thus

$$\Phi = kL + \beta_{lp} = q\pi, \quad (19)$$

where q is the number of half-wavelengths of the axial standing-wave pattern.

In general, the kernel in Eq. (16) is symmetric but not Hermitian; therefore the eigenvalues γ_{lp} are complex and the existence of a complete set of eigenfunctions cannot be guaranteed in advance. The eigenfields are not power orthogonal in the usual sense; rather, they are biorthogonal.²¹

B. Numerical Considerations

We have employed two methods to solve Eq. (16). The first one is a matrix method that consists of converting the round-trip integral equation into a matrix eigenvalue equation.^{22,23} This method makes use of a Gauss–Legendre quadrature rule and has some important advantages: It extracts the lowest N modes and eigenvalues at the same time, its accuracy is determined by the size N of the matrix,¹⁵ and it can handle the case of closely spaced eigenvalues that is a difficult task for iterative methods. The second method is the classical Fox–Li iterative scheme.¹⁷ This method extracts the dominant or the lowest-loss eigenmodes, but, as already mentioned, it is inefficient near eigenvalue degeneracies. The Fox–Li method has the advantage that for cylindrical symmetries, the kernels in Eqs. (12) and (13) resemble a Hankel transform and, as a consequence, it is possible to use fast algorithms for propagating each radial eigenmode and eigenvalue in the resonator.²⁴

Typically the value of the radial coordinate is bounded by a maximum value where the input and output fields are small enough to be neglected; otherwise it is bounded by the radius a_1 of the double axicon. Let $\mathbf{r} = [r_1, r_2, \dots, r_N]$ and $\mathbf{w} = [w_1, w_2, \dots, w_N]$ be the abscissas and weight factors for Gauss–Legendre quadrature in the range $(0, a_1)$. If $\mathbf{u}_{lp} = [u_1, u_2, \dots, u_N]$ is a column vector representing the eigenfield evaluated at radius \mathbf{r} , then Eq. (16) takes the matrix form

$$\gamma \mathbf{u}_{lp} = (\mathbf{H} * \mathbf{W}) * \mathbf{u}_{lp}, \quad (20)$$

where \mathbf{H} is a $N \times N$ matrix with elements $H_{m,n} = H(r_m, r_n)$ and \mathbf{W} is a diagonal matrix with elements $[w_1, w_2, \dots, w_N]$.

The matrix product $\mathbf{H} * \mathbf{W}$ corresponds to the propagation matrix from plane 1 to plane 3. Since we are breaking up the round-trip propagation by performing two plane-to-plane propagations, this product can be seen as the product of two propagation matrices \mathbf{P}_{12} and \mathbf{P}_{23} corresponding to the equivalent matrix representation for the propagation integrals of Eqs. (12) and (13) respectively. Equation (20) can be rewritten as

$$\gamma \mathbf{u}_{lp} = (\mathbf{P}_{23} * \mathbf{P}_{12}) * \mathbf{u}_{lp}, \quad (21)$$

where $\mathbf{P}_{m,n} = \mathbf{H}_{m,n} * \mathbf{W}$. The eigenvalues and eigenvectors of Eq. (21) can be easily extracted using the well-known matrix eigenvalue algorithms.

C. Resonating Modes

The physical parameters for the resonator used in our calculations correspond to typical values of a gas-discharge, fast axial flow cw CO₂ laser resonator: aperture size of the axicon $a_1 = 10$ mm, $n = 2.4$ (corresponding to commercially available zinc selenide axicons), axicon wedge angle $\alpha = 0.5^\circ$, and wavelength $\lambda = 10.6$ μm . The radius of the output mirror is chosen to be $a_2 = 5$ mm.

From approximation (1) the values for the cavity length and apex angle are calculated, yielding $L = 40.92$ cm and $\theta_0 = 12.22 \times 10^{-3}$ rad. A 200-point Gauss–Legendre quadrature was used to solve Eq. (21).

To make appropriate comparisons, we consider first the fundamental mode $(l, p) = (0, 1)$ of the resonator with plane output mirror (i.e., $R \rightarrow \infty$). Figure 2 shows the amplitude and phase of the transverse profiles at both the axicon plane (RP₁=RP₃) and output mirror (RP₂). The eigenfield and the eigenvalue at the axicon plane were determined by using the matrix method described in Subsection 3.B. As stated in Section 2, the field at the output mirror corresponds to an ideal zeroth-order Bessel beam $J_0(k, \rho)$ modulated by a bell-shaped amplitude function. The modulation of the output beam is evident from the comparison with the theoretical Bessel beam shown in

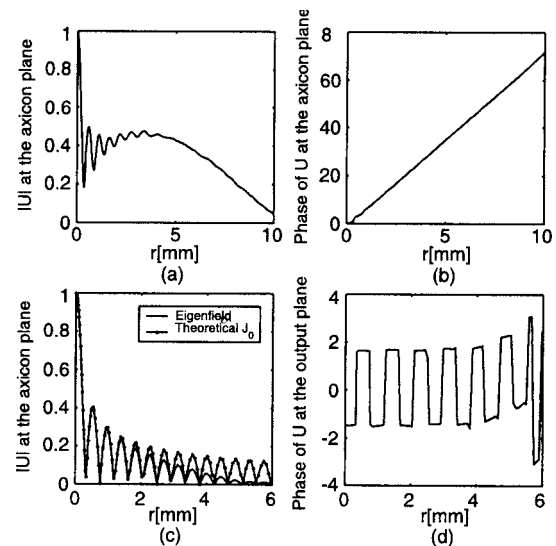


Fig. 2. Transverse profiles of the magnitude and phase of the fundamental Bessel mode at (a), (b) the axicon plane and (c), (d) the output plane for a resonator with output flat mirror and $a_2 = 5$ mm.

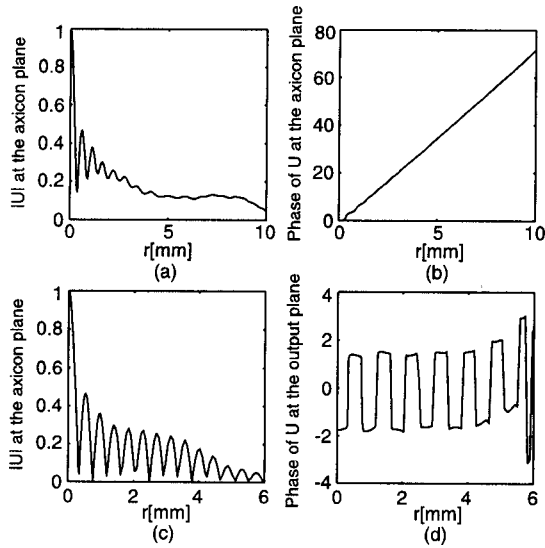


Fig. 3. Transverse profiles of the magnitude and phase of the fundamental Bessel mode at (a) (b) the axicon plane and (c) (d) the output plane for a UBR with $R=-50L$ and $a_2=5$ mm.

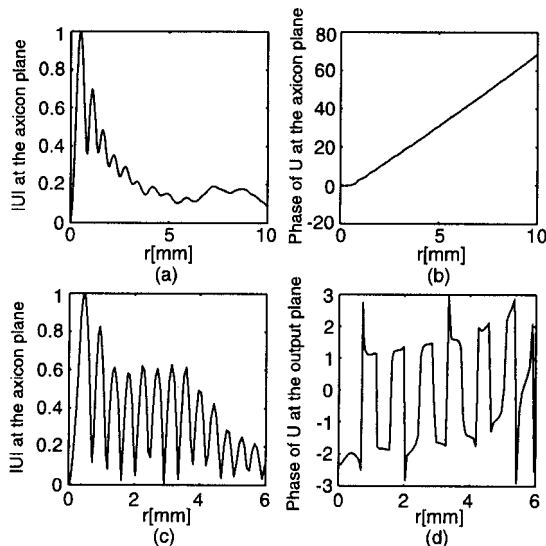


Fig. 4. Transverse profiles of the magnitude and phase of the second-order Bessel mode at (a), (b) the axicon plane and (c), (d) the output plane for a UBR with $R=-50L$ and $a_2=5$ mm.

Fig. 2(c). It can easily be seen how the amplitude of the output beam decreases near the edge of the output mirror. For the range $[0, 3$ mm] the plots are very similar and almost overlap such that differences are negligible. In Fig. 2(b) we see that the phase of the field is almost linear with slope $k\theta_0$; this fact confirms that the field at the axicon behaves as a conical wave.

Let us now consider the case of the UBR. We replace the plane output mirror by a convex-spherical mirror with radius of curvature $R=-50L$. The amplitude and phase of the fundamental mode at both the axicon plane (RP₁) and just before the output mirror (RP₂) are depicted in Fig. 3. Note that the radial variation of the output field [shown in Fig. 3(c)] still resembles closely a Bessel beam whose rings preserve the same separation as is the case for $R \rightarrow \infty$ shown in Fig. 2. This result is in agreement

with the fact that the ring separation is determined by the characteristic angle of the conical mirror only, namely, we have $k_t = k \sin \theta_0 \approx k \theta_0$; thus the separation between consecutive Bessel fringes is $\theta_0/2\lambda$. As expected, the phase just before the axicon plane behaves linearly according to $k\theta_0 r$.

Higher-order solutions u_{lp} and γ_{lp} for Eq. (16) can also be obtained. When the output coupler is plane, the ideal transverse field is given by Eq. (2). Figure 4 shows the magnitude and phase of the eigenfield corresponding to the second-order $(l,p)=(2,1)$ for a radius of curvature $R=-50L$ at the axicon and output planes.

D. Intracavity Field Distribution

The classical Fox and Li iteration method was implemented to determine numerically the passive three-dimensional field structure of the cavity modes. For this purpose, the diffractive field calculations are based on the angular spectrum of the plane-waves representation utilizing the fast-Fourier-transform algorithm. The transverse field is sampled in the reference plane over a grid of 512×512 points. Typically around 150 round trips are required for the process to converge, starting from an arbitrary field distribution. The three-dimensional intracavity field distribution was obtained by calculating the field at 200 transverse planes evenly spaced through the unfolded cavity.

The intracavity field distribution of the dominant lowest-order mode in the UBR with convex output mirror ($R=-50L$) is presented in Fig. 5. Forward propagation goes from the axicon plane at $z=0$ to the output mirror plane at $z/L=1$. Reverse propagation goes from the output mirror at $z/L=1$ to the axicon plane at $z/L=2$. The axicon and the output mirror extend in transverse dimension from -1 to 1 and from -0.5 to 0.5 in normalized units r/a_1 , respectively. The corresponding transverse fields at the axicon and output mirror planes were already calculated through eigenequation (16) and depicted in Fig. 3.

The results shown in Fig. 5 clearly illustrate the conical nature of the field within the cavity. At the middle plane of the axicon, the field is approximately a plane wave; after crossing the axicon, the diffraction pattern of the conical wave exhibits a bright-line focus surrounded by a series of cylindrical concentric sidelobes with gradually

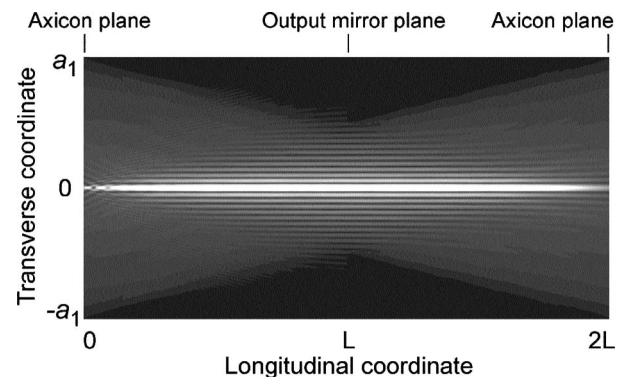


Fig. 5. Passive three-dimensional intracavity field distribution in the UBR with $R=-50L$. The eigenfield is first forward propagated from the axicon plane to the output plane and later returned backward to the axicon plane.

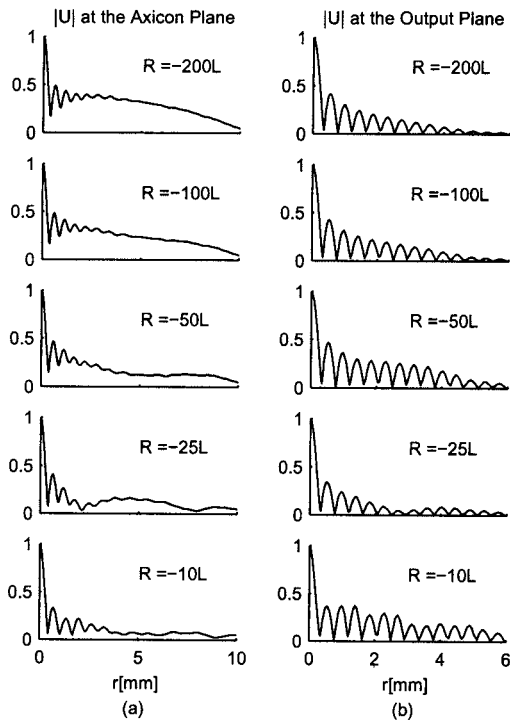


Fig. 6. Transverse profiles of the magnitude of the fundamental Bessel mode at the axicon and output planes of the UBR for several ratios R/L .

diminishing intensity. We performed a number of Fox–Li simulations for a variety of initial conditions, including uniform plane waves, Gaussian profiles with different widths, and random noisy transverse patterns. Regardless of the initial condition, the field always converged to the dominant mode of the cavity with the expected profile and radial frequency characteristics imposed by the geometrical parameters.

4. ANALYSIS OF THE DIFFRACTIVE LOSSES AND FREQUENCY SHIFTS

From a practical point of view, it is of great interest to study the effect of varying the resonator parameters. The relevant output characteristics are the transverse field profile, the diffractive loss, and the resonant frequency shift.

A. Effect of Varying the Radius of Curvature of the Output Coupler

The effect of varying the radius of curvature of the output mirror on the field distribution at the axicon and output planes is shown in Fig. 6. For $R = -200L$ there exist few differences between the fundamental eigenmode of the resonator and the ideal Bessel beam shown in Fig. 2. As R decreases, the transverse field at the axicon plane tends to concentrate around the vertex of the conical mirror, and the Bessel rings are modulated by a radial amplitude factor. Note that the ring separation remains constant under the variation of R . The output radial distribution of the J_2 Bessel mode for several radii of curvature is depicted in Fig. 7. One can see that the calculated eigenfields are multiringed and that as R increases the pattern

becomes more similar to a theoretical second-order Bessel beam. Note that higher-order modes experience the same radial modulation as the fundamental mode.

We consider now the loss behavior corresponding to the lower-order modes resonating within the UBR. The loss Γ_{01} for the fundamental mode is depicted in Fig. 8(b) as a function of the normalized radius R/L for two different

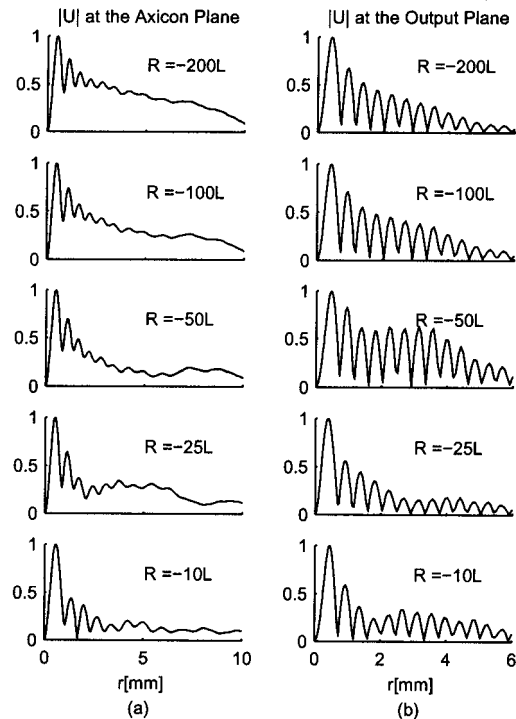


Fig. 7. Transverse profiles of the magnitude of the second-order Bessel mode at the axicon and output planes of the UBR for several ratios R/L .

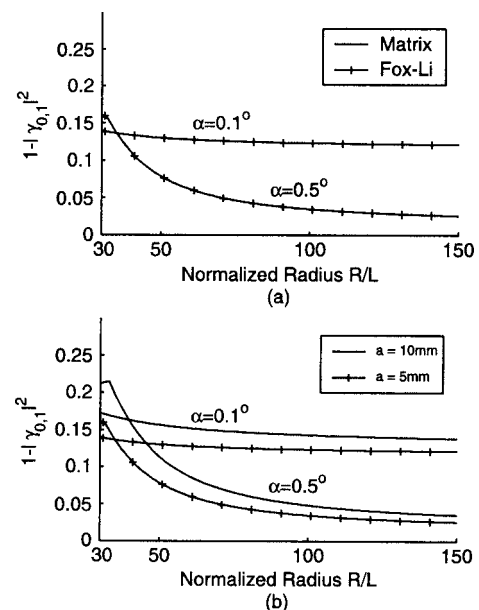


Fig. 8. (a) Diffractive losses $\Gamma = 1 - |\gamma|^2$ in terms of the normalized radius R/L for the fundamental mode with different wedge angles. Comparison of results with the matrix and Fox–Li methods. (b) Comparison of the results for different aperture sizes of the output mirror.

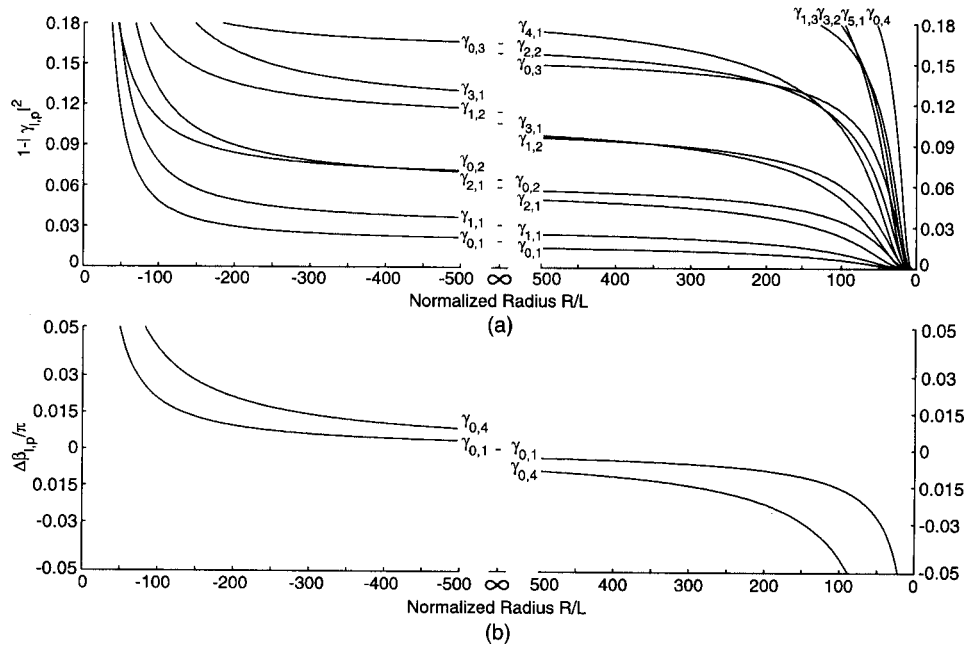


Fig. 9. Transition between the stable and the unstable regions of the Bessel resonator. (a) Diffraction losses $\Gamma = 1 - |\gamma|^2$ and (b) normalized phase shifts $\Delta\beta/\pi$ are depicted as a function of the normalized radius R/L . Mode crossings are present for higher-order modes. In (b) the phase curves for the considered modes in (a) are contained within the region between the phase curves for modes (0,1) and (0,4).

Table 1. Diffraction Losses for the First Ten Modes

$R = -50L$		$R \rightarrow \infty$		$R = 50L$	
Mode	Loss	Mode	Loss	Mode	Loss
0,1	0.11346	0,1	0.0178	0,1	0.00207
1,1	0.16585	1,1	0.0302	1,1	0.00376
0,2	0.16826	2,1	0.0593	2,1	0.00866
0,3	0.21633	0,2	0.0633	0,2	0.01745
1,2	0.24841	1,2	0.1072	3,1	0.02057
2,1	0.25777	3,1	0.1132	1,2	0.03146
1,3	0.28333	0,3	0.1583	4,1	0.04722
5,1	0.28878	2,2	0.1720	2,2	0.06103
6,1	0.29033	4,1	0.1984	0,3	0.07725
4,1	0.29376	1,3	0.2216	5,1	0.09664

values of the axicon wedge angle α and for two different values of the output mirror radius a_2 . These plots were computed by finding the eigenvalues from Eq. (16) for a large number of radii of curvature in the range $-200 < R/L < -30$ and were also corroborated by using the Fox-Li algorithm [+ symbols Fig. 8(a)].

There are some conclusions that can be inferred from the curves in Fig. 8(a): In general, the mode loss increases as the output mirror becomes more and more convex, loss increases as the aperture diameter of the output mirror a_2 moves away from the value $a_1/2$, and loss increases as the axicon wedge angle decreases. It has been found that the lowest-loss curve occurs when the value of the output aperture is $a_2 \approx a_1/2$.

It is expected that the resonant frequency of a particular resonating mode in the UBR will change if the value of R changes. The resonant frequency can be written as $\nu = \nu_\infty + \Delta\nu$, where ν_∞ is the resonance frequency of the reso-

nator with the plane output mirror and $\Delta\nu$ is the frequency shift introduced by the variation of the radius of curvature. Let us now define the relative phase shift experienced by a resonating mode inside the cavity as $\Delta\beta = \beta(R) - \beta_\infty$, with $\beta(R)$ being the phase angle of the corresponding eigenvalue in terms of R and β_∞ the angle for the case when $R \rightarrow \infty$, i.e., plane output mirror.

The frequency shift $\Delta\nu$ in terms of the phase shift $\Delta\beta$ is found to be

$$\Delta\nu = -\nu_0(\Delta\beta/\pi), \tag{22}$$

where $\nu_0 = c/2L$ is the fundamental beat frequency, i.e., the frequency spacing between successive longitudinal resonances. Figure 9(b) illustrates the normalized phase shift $\Delta\beta/\pi$ for the first four azimuthal modes $l = (0,1,2,3)$ and $p=1$. It is readily evident from these

curves that the resonant frequency increases as the output coupler becomes more convex.

B. Transition between the Unstable and Stable Bessel Resonators

In Fig. 9 we show the eigenvalue spectrum of the UBR and the SBR as a function of the normalized radius of curvature R/L . Numerical values are included in Table 1 for the first ten modes sorted in ascending order by loss for the UBR ($R=-50L$), the SBR ($R=50L$), and the resonator with a plane output mirror ($R \rightarrow \infty$). The plots in Fig. 9 clearly illustrate that the transition between the UBR and the SBR is characterized by a continuous change in the associated diffraction losses and frequency shifts. These results were determined from matrix equations (21) taking equal diameters for the axicon and the output mirror. The loss curves of all modes exhibit a monotonically increasing behavior as the output mirror becomes more convex. This result is expected from the fact that in the SBR the field is constantly refocused by the concave mirror and the axicon, whereas in the UBR only the axicon forces the field to propagate toward the optical axis. Note that mode crossing points are present for higher modes. In Fig. 10 we compare the output field profiles of the SBR and the UBR for the J_0 and the J_2 Bessel modes. Whereas the SBR retains a Gaussian radial modulation on the Bessel rings, the UBR exhibits a more uniform modulation.

C. Effect of Changing the Cavity Length

The relationship in approximation (1) between the cavity parameters shown in Fig. 1 seems to be restrictive. To study the effect of varying the cavity length, let us first define the length factor $\mu=L/L_0$, where L_0 is the unchanged cavity length in approximation (1) and L is the current length. The fundamental mode patterns at the

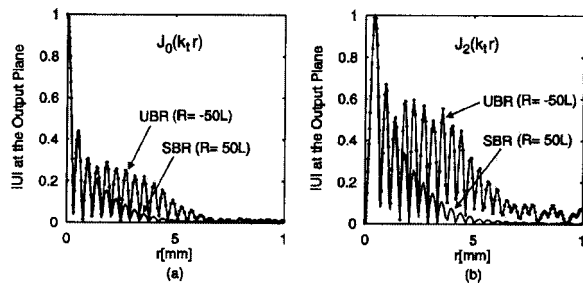


Fig. 10. Comparison between the transverse modes for the SBR and the UBR.

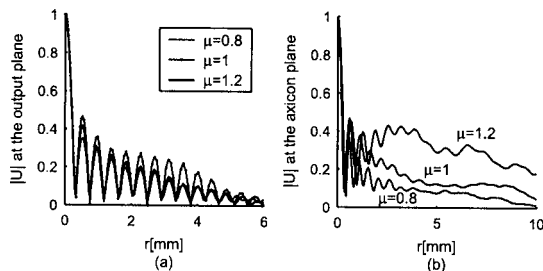


Fig. 11. Transverse field patterns at the output and axicon planes corresponding to the length factors $\mu=0.8, 1$, and 1.2 for convex output mirror with $R=-50L$ and $\alpha=0.5$.

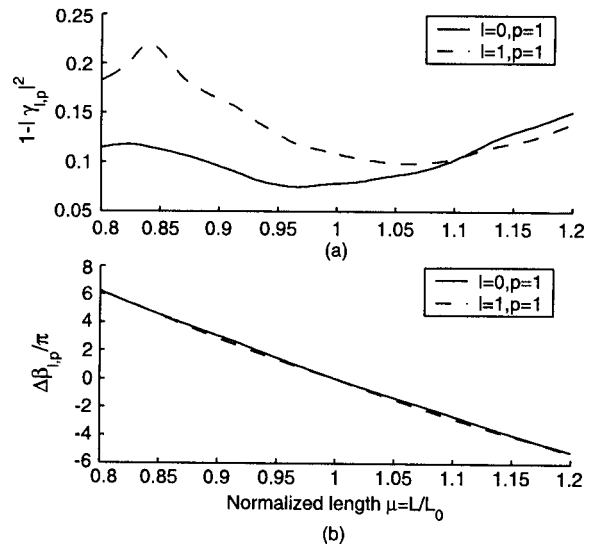


Fig. 12. Loss and resonant frequency shift behavior as a function of the length factor μ for the first two angular modes $(l,p)=(0,1)$ and $(1,1)$, with $R=-50L$ and $\alpha=0.5$.

axicon and the output mirror planes are depicted in Fig. 11 for $\mu=[0.8, 1.0, 1.2]$. Note that the radial separation of the Bessel rings remains practically constant, which means that the transverse component of the propagation vector is not affected by a change in the cavity length. The main difference between the profiles shown in Fig. 10 is related to diffraction losses. We can see that the modes for $\mu=0.8$ and 1.2 present larger losses than the mode for $\mu=1$; therefore it is expected that the amplitudes of their output profiles decrease faster.

The curve for the losses is depicted in Fig. 12(a) for the first two azimuthal modes ($l=0, 1$) and $R=-50L$. As in the case reported for the SBR,¹⁵ it is remarkable that the minimum for the loss curves does not occur at the value of $\mu=1$ as expected, but at a slightly different value of μ . For the fundamental mode $(0, 1)$ it occurs at $\mu \approx 0.958$, whereas for mode $(1, 1)$ it is ~ 1.035 . Note that mode $(1, 1)$ becomes the fundamental mode of the resonator as the cavity length increases; this mode crossing due to the varying cavity length also occurs between other higher-order modes.

Figure 12(b) depicts the relative phase-shift behavior for $l=0$ and 1 . We redefined the relative phase shift now in terms of the length L as $\Delta\beta=\beta(L)-\beta_{L_0}$, where $\beta(L)$ is the phase angle of the eigenvalue as a function of the varying length and β_{L_0} is the angle for the cavity length given by approximation (1). It can be readily seen that the relative phase-shift behavior is almost linear and that it decreases for an increasing μ .

5. CONCLUSIONS

A detailed analysis of the resonating modes in the axicon-based unstable Bessel resonator with a spherical-convex output mirror has been presented. We studied the mode behavior under the variation of the radius of curvature of the output coupler, the axicon angle, and the cavity length, taking into account the finite aperture size of the

mirrors composing the cavity. The most important conclusions are summarized as follows:

- UBRs support higher-order Bessel-like modes that satisfy a biorthogonal relation rather than an orthogonal relation.
- The eigenvalue matrix method, based on the discretization of the Huygens–Fresnel self-consistency equation, is particularly useful for extracting the first N eigenfields and eigenvectors (i.e., losses and frequency shifts) of the resonating modes at the output coupler and the axicon plane of the UBR. The Fox–Li algorithm was used to extract the dominant mode of the cavity, obtaining an excellent agreement with the matrix method.
- UBRs possess higher transverse-mode discrimination in favor of the fundamental mode than SBRs.
- While the SBR retains a Gaussian radial modulation on the Bessel rings, the UBR exhibits a more uniform amplitude modulation that produces output profiles more similar to ideal Bessel beams. It now seems clear that for a laser system characterized by a least moderate gain per pass (50% per pass), the best practical cavity for obtaining nearly ideal Bessel beams will be a UBR with $R = -50L$.
- Given the light wavelength, the radial separation of the Bessel rings in the UBR depend only on the characteristic angle of the conical mirror.
- The transition between the UBR and the SBR is characterized by a continuous change in the associated diffraction losses and frequency shifts.
- In general, the mode loss increases as the output mirror becomes more convex, and the loss increases as the axicon wedge angle decreases. The lowest-loss curve occurs when the value of the aperture radius of the output coupler is $a_2 \approx a_1/2$.
- The mode $(l, p) = (0, 1)$ exhibits the lowest-loss curve for practically all values of the radius of curvature of the output mirror; mode crossing points are, however, present for higher modes.
- The mode (1,1) becomes the fundamental mode of the resonator as the cavity length increases beyond ~ 1.15 times the unchanged cavity length defined by approximation (1). Mode crossing points due to the varying cavity length also occur between other higher-order modes.
- The cavity loss for the fundamental mode is minimized when the cavity length is $\sim 96\%$ of the value predicted by geometrical optics.
- The reduction of the aperture size of the output convex mirror reduces edge-diffraction effects and prevents significant energy spillage across the vertex of the axicon mirror.

The analysis presented in this paper consolidates previous works on the production of Bessel and Bessel–Gauss beams in laser resonators.^{13–16}

ACKNOWLEDGMENT

The authors acknowledge financial support from Conacyt–México grant 42808 and from the Tecnológico de Monterrey Research Chair in Optics grant CAT-007.

Corresponding author Julio C. Gutiérrez-Vega can be reached by e-mail: at juliocesar@itesm.mx.

REFERENCES

1. J. Durnin, “Exact solutions for nondiffracting beams. I. The scalar theory,” *J. Opt. Soc. Am. A* **4**, 651–654 (1987).
2. J. Durnin, J. J. Micely, Jr., and J. H. Eberly, “Diffraction-free beams,” *Phys. Rev. Lett.* **58**, 1499–1501 (1987).
3. G. Indebetouw, “Nondiffracting optical fields: some remarks on their analysis and synthesis,” *J. Opt. Soc. Am. A* **6**, 150–152 (1989).
4. G. Scott and N. McArdle, “Efficient generation of nearly diffraction-free beams using an axicon,” *Opt. Eng. (Bellingham)* **31**, 2640–2643 (1992).
5. J. Turunen, A. Vasara, and A. T. Friberg, “Holographic generation of diffraction-free beams,” *Appl. Opt.* **27**, 3959–3962 (1988).
6. A. Vasara, J. Turunen, and A. T. Friberg, “Realization of general nondiffracting beams with computer-generated holograms,” *J. Opt. Soc. Am. A* **6**, 1748–1754 (1989).
7. Z. L. Horváth, M. Erdélyi, G. Szabó, Zs. Bor, F. K. Tittel, and J. R. Cavallaro, “Generation of nearly nondiffracting Bessel beams with a Fabry–Perot interferometer,” *J. Opt. Soc. Am. A* **14**, 3009–3013 (1997).
8. W.-X. Cong, N.-X. Chen, and B.-Y. Gu, “Generation of nondiffracting beams by diffractive phase elements,” *J. Opt. Soc. Am. A* **15**, 2362–2364 (1998).
9. J. Durnin and J. H. Eberly, “Diffraction free arrangement,” U.S. patent 4,887,885 (December 19, 1989).
10. K. Uehara and H. Kikuchi, “Generation of nearly diffraction-free laser beams,” *Appl. Phys. B* **48**, 125–129 (1989).
11. P. Pääkkönen and J. Turunen, “Resonators with Bessel–Gauss modes,” *Opt. Commun.* **156**, 359–366 (1998).
12. A. Hakola, S. C. Buchter, T. Kajava, H. Elfström, J. Simonen, P. Pääkkönen, and J. Turunen, “Bessel–Gauss output beam from a diode-pumped NdYAG laser,” *Opt. Commun.* **238**, 335–340 (2004).
13. J. Rogel-Salazar, G. H. C. New, and S. Chávez-Cerda, “Bessel–Gauss beam optical resonator,” *Opt. Commun.* **190**, 117–122 (2001).
14. A. N. Khilo, E. G. Katranji, and A. A. Ryzhevich, “Axicon-based Bessel resonator: analytical description and experiment,” *J. Opt. Soc. Am. A* **18**, 1986–1992 (2001).
15. J. C. Gutiérrez-Vega, R. Rodríguez-Masegosa, and S. Chávez-Cerda, “Bessel–Gauss resonator with spherical output mirror: geometrical and wave-optics analysis,” *J. Opt. Soc. Am. A* **20**, 2113–2122 (2003).
16. C. L. Tsangaris, G. H. C. New, and J. Rogel-Salazar, “Unstable Bessel beam resonator,” *Opt. Commun.* **223**, 233–238 (2003).
17. A. G. Fox and T. Li, “Resonant modes in a maser interferometer,” *Bell Syst. Tech. J.* **40**, 453–488 (1961).
18. A. E. Siegman, *Lasers* (University Science, 1986).
19. B. Lissak and S. Ruschin, “Transverse pattern modifications in a stable apertured laser resonator,” *Appl. Opt.* **29**, 767–771 (1990).
20. B. Duszcyk, M. P. Newell, and S. J. Sugden, “Numerical methods for solving the eigenvalue problem for a positive branch confocal unstable resonator,” *Appl. Math. Comput.* **140**, 427–443 (2003).
21. A. E. Siegman, “Unstable optical resonators,” *Appl. Opt.* **13**, 353–367 (1974).
22. W. D. Murphy and M. L. Bernabe, “Numerical procedures for solving nonsymmetric eigenvalue problems associated with optical resonators,” *Appl. Opt.* **17**, 2358–2365 (1978).
23. W. P. Latham, Jr., and G. C. Dente, “Matrix methods for bare resonator eigenvalue analysis,” *Appl. Opt.* **19**, 1618–1621 (1980).
24. M. Guizar-Sicairos and J. C. Gutiérrez-Vega, “Computation of quasi-discrete Hankel transforms of integer order for propagating optical wave fields,” *J. Opt. Soc. Am. A* **21**, 53–58 (2004).